Torregrosa, AJ.; Payri, R.; Salvador, FJ.; Crialesi-Esposito, M. (2020). Study of turbulence in atomizing liquid jets. International Journal of Multiphase Flow. 129:1-12. https://doi.org/10.1016/j.ijmultiphaseflow.2020.103328

# Study of turbulence in atomizing liquid jets

Antonio J. Torregrosa, Raúl Payri, F. Javier Salvador, Marco Crialesi-Esposito*

*CMT-Motores Térmicos, Universitat Politècnica de València, Spain.*

**Abstract**

Among the many unknowns in the study of atomizing sprays, defining an unambiguous way to analyze turbulence is, perhaps, one of the most limiting ones. The lack of proper tools for the analysis of the turbulence field (e.g. specific one/two-point statistics, spectrum, structure functions) limits the understanding of the overall phenomenon occurring, impeding the correct estimation of motion scales (from the Kolmogorov one to the integral one). The present work proposes a methodology to analyze the turbulence in atomizing jets using a pseudo-fluid method. The many challenges presented in these types of flows (such as temporal fluid properties uncertainties, strong anisotropy and lack of a priori chance of determining the motion scales) can be simplified by such a method, as it will be clearly shown by the smooth results obtained. Finally, the method is tested against the one-phase flows turbulent data available in the literature for the Kolmogorov scaling of the one-dimension energy spectra, showing how a pseudo-fluid method could provide a reliable tool to analyze multiphase turbulence, especially in spray's primary atomization.

*Keywords:* Energy spectra, pseudo-fluid, turbulence, primary atomization, Kolmogorov scale.

## 1. Introduction

Atomizing sprays are a fundamental process in many applications, ranging from the fuel injection in combustion chambers Manin (2019), pharmaceutical applications Aliseda et al. (2008) and food industry applications Lasheras and Hopfinger (2000). Depending on the resulting flow composition, in terms of droplet size, distribution and penetration, various type of atomizers can be used, as for example plain nozzle, coaxial injection of both liquid and gas, sheet atomizers just to name a few (a detailed recompilation of atomizers type can be found in Lefèbvre et al. (1989)). It is well established, both in physics and within the industrial sector, that turbulence is one of the main causes for the breakup of liquid structures but its behavior is still eluding our knowledge. In fact, while tools for the analysis of single phase turbulence are growing more and more (and so our knowledge on this phenomena), the analysis of turbulence in multiphase flows has no established theory to rely on and no specific knowledge is provided on this regard.

There has been, mainly during the last decade, a significant growth regarding the analysis of turbulence in multiphase flows, mostly given by the rise of Direct Numerical Simulations (DNS) performed thanks the continuously improved computational resources available. A remarkable contribution was provided by Lucci et al. (2010), where he studied, using DNS of Homogeneous Isotropic Turbulence (HIT), a particle laden flow composed of solid particles by the size of the Taylor lengthscale. In this work the authors observe, by means of the flow spectra, how the turbulent structures in the inertial subrange are "broken up" by the droplets, generating a spectra deviation associated with higher energy content at smaller scales. These findings were also supported by the results presented in Dodd and Ferrante (2016) for droplet laden flows in HIT simulated using DNS. This work constitutes a very important contribution in the analysis of turbulence in multiphase flows and is, in the authors opinions, technically very sound. However both Lucci et al. (2010); Dodd and

*Corresponding author
*Email address:* marcres@mot.upv.es (Marco Crialesi-Esposito)

Ferrante (2016) are limited to HIT scenarios that, while very useful for theoretical studies, are difficult to relate to a turbulent spray, due to the strong anisotropy in the injection direction. Furthermore, primary atomization is obviously neglected, while in Dodd and Ferrante (2016) secondary breakup is still possible. The absence of the typical variety of droplet sizes that has been observed in primary atomization Ling et al. (2017); Marmottant and Villermaux (2004); Wang and Bourouiba (2018) does not allow for an estimation of the effects of droplets over the energy spectra that may be useful for atomization studies.

HIT DNS simulations were also performed in Duret et al. (2011) where quite different results were obtained. Here the spectral analysis (performed in a separated fashion for each phase) shows that the phase with the higher percentage of volume fraction tends to behave as single-flow turbulence (e.g. verifying the -5/3 law). This result is substantially different when compared to Dodd and Ferrante (2016). In the authors opinion, this may relate to the different conditions in which the flows were initialized. In fact, while in Dodd and Ferrante (2016) the initial droplet size was strictly controlled, in Duret et al. (2011) the liquid phase is composed of liquid structures of different shape and volumetric diameter, hence no specific wavelength (e.g. the droplet diameter in Dodd and Ferrante (2016)) marks the presence of the multiphase nature of the flow. Furthermore, the HIT in Duret et al. (2011) is maintained, while in Dodd and Ferrante (2016) is decaying, increasing the relevance of droplet insertion in the domain and limiting the breakup-coalescence events. A detailed and exhaustive review on the topic of droplet/bubbles laden flows is provided in Elghobashi (2018), while a interesting comparison on various numerical methods and their effects on the energy spectra is provided in Brändle de Motta et al. (2019).

The complexity of the analysis of turbulence in atomizing flows lies also in the anisotropic nature of the flows and in the a-priori uncertainties related to droplet distributions, flow behavior (both on the average and the turbulent components) and characteristic scales. Many a-posteriori analysis of atomizing flows have been performed, by means of DNS, during the very last years. In the recent work of Ling et al. (2019), the authors studied a a coflow planar jet atomizer and performed a detailed analysis of the turbulence field, going from the spatial and temporal spectrum to the energy balance. In this work also a first attempt has been performed to compute the typical scales of atomizing flows, such as the Kolmogorov scale and the Hinze scale Hinze (1955). Of particular interest is also the analysis of the energy dissipation rate convergence over simulations with different levels of refinements, which suggests the quality of the simulation performed, as well as the inherent capability of multiphase flows to dissipate small eddies on the liquid surface (hence improving simulation convergence for unrefined simulations).

Recently, Hasslberger et al. (2019) performed a topological analysis of the turbulence in an atomizing liquid jet (as the case studied in this work). In this work, the authors performed an analysis on the probability distribution of topology islands, while the determination of the Kolmogorov scale is interestingly performed a-priori. Another interesting approaches is proposed in Zandian et al. (2018), where a vorticity-based analysis method is used to understand how the turbulence, generated by the Kelvin-Helmholtz instability, is interacting with surface instabilities and breakup events. While this method may be very interesting to assess a phenomenological model for breakup, its usage for understanding primary atomization is, somehow, more academical while, on the other hand, allows to isolate the effects of one main instability. Similar approach was followed by Shinjo and Umemura (2010) in one of the largest DNS simulations of round atomizing jet published.

In this work, a DNS study of the turbulence generated by the atomization process based on the pseudo-fluid approach is proposed. A significant effort will be put in achieving smooth statistics, which consequently implies rather long simulation times. While the methods for computing one-point statistics will be proposed and analyzed, a significant focus will be put on the spectral analysis of the flow. The reason behind this choice can be found in Gorokhovski and Herrmann (2008); Villermaux (2007), where the theory of fragmentation, discussed by Kolmogorov Kolmogorov (1941), is presented. Fragmentation has also been strictly related via many works to the energy cascade, therefore it is likely that both liquid structures and turbulent structures breakups develop in similar fashions. It is therefore important to understand how the energy cascade develops for primary atomization in liquid jets, if and how it deviates from the single phase energy cascade and finally whether or not a pseudo fluid approach may be a feasible mathematical description of turbulence, so that physical insight can be drawn from this type of DNS simulation approach.

## 2. Methodology

### *2.1. Governing Equations and Numerical Methods used*

For this study the open source code ParisSimulator has been used. While the main features of this code has been highlighted in several works Ling et al. (2017); Aniszewski et al. (2018); Hasslberger et al. (2019) here a brief description of the methodologies used in this work will be presented. The code is written in Fortran90 and parallelized using MPI (for the simulation described in this work, 4096 cores were used). It uses the one-fluid formulation of the incompressible Navier-Stokes equation, solved over a cartesian mesh with staggered grid. The Navier-Stokes equation and the mass conservation equation are solved in their form:

$$\nabla \cdot \mathbf{u} = 0 \tag{1a}$$

$$\rho(\partial_t \mathbf{u} + \mathbf{u} \cdot \nabla \mathbf{u}) = -\nabla p + \nabla \cdot [\mu \left(\partial_i u_j + \partial_j u_i\right)] + \sigma \kappa \delta_s \mathbf{n}. \tag{1b}$$

Obviously, for incompressible flows, the velocity field $\mathbf{u}$ results into a divergence-free field in the mass conservation in Equation (1a). In Equation (1b), $\rho$ is the fluid density, $\mu$ is the fluid kinematic viscosity and $p$ is the pressure. The last term in Equation (1b) RHS is the effect produced by the surface tension, $\sigma$: the surface normal is $\mathbf{n}$ and the liquid surface curvature $\kappa$ is computed using the Height-Function, proposed by Popinet (2009). The surface force term is finally concentrated on the liquid interface by using a Dirac delta function $\delta_s$.

The advection term is discretized using a third-order quadratic upstream interpolation for convective kinematics (QUICK) method while the momentum diffusion term is computed using a second order central differencing scheme. The divergence free condition is imposed using the Chorin projection method Chorin (1968) for computing the velocity during a second-order predictor-corrector time integration.

The one-fluid method allows to compute the fluid properties at each position by using a color function $C$ within an arithmetic mean between the gas and the liquid properties, such as:

$$\rho(\mathbf{x}) = \rho_l C + \rho_g (1 - C) \tag{2a}$$

$$\mu(\mathbf{x}) = \mu_l C + \mu_g (1 - C) \tag{2b}$$

where the subscripts $l$ and $g$ are respectively referring to the liquid and the gas phase. The color function marks the composition of the fluid within the cell, being $C = 1$ only liquid phase and $C = 0$ only gas phase, as it can be deduced from Equation (2). The advection of the color function is then computed as:

$$\partial_t C + u_i \partial_i C = 0. \tag{3}$$

Equation (3) is computed using the Volume of Fluid (VOF) method and solved using the numerical scheme *Calcul d'Interface Affine par Morceaux* (CIAM) presented in Scardovelli and Zaleski (2003).

### *2.2. Simulation design*

In a first place, the physical parameters for the simulation and the fluid properties have been selected so that the simulation can be compared against previous results Salvador et al. (2018) and are reported in Table 1. Here, $\langle U \rangle$ is the average bulk injection velocity, $D_n$ is the nozzle diameter and $Re_b$ is the Reynolds computed with the bulk velocity (the reason for such choice can be found in Salvador et al. (2018)).

As previously discussed, a significant effort in this paper is put into a providing reliable and convergent statistics. This consideration limits the amount of cells used to solve the problem. While this has obviously a significant impact on the amount of turbulent energy resolved Pope (2001) a perfect resolution of all the motion and breakup scales has not yet been achieved and is not foreseen with current computer capabilities Ling et al. (2017). On the other hand, this simulation still aims at resolving wavelengths well within

| $Re_b$ | $\rho_l$ | $\rho_g$ | $\mu_l$ | $\mu_g$ | $\sigma$ | $\langle U \rangle$ | $D_n$ |
|---|---|---|---|---|---|---|---|
| 5037 | 750 | 22.8 | $1.34 \cdot 10^{-3}$ | $1.85 \cdot 10^{-5}$ | $2.53 \cdot 10^{-2}$ | 100 | 90 |
| - | $kg/m^3$ | $kg/m^3$ | $Pa \cdot s$ | $Pa \cdot s$ | $N/m$ | $m/s$ | $\mu m$ |

Table 1: Physical simulation properties for the case studied.

the dissipative range. Furthermore, based on the knowledge provided in previous studies Salvador et al. (2018), the domain in directions normal to the spray centerline should be as large as possible, so that the larger eddy (formed during the spray penetration transient) is able to properly been resolved within the simulation domain (meaning that the domain extreme points' velocities do not correlate with the velocity field generated within the eddy). With these considerations in mind, the simulation parameters, both for the time and space resolution are proposed in Table 2, where $l_i$ is the domain length in the i-th direction, $dx$ and $dt$ are respectively the mesh size and the time step. A few words should be dedicated to $T_t$ and $T_{ss}$, which are respectively the transient time (the time that the spray tip needs to reach outgoing the domain in the streamwise direction) and the statistically stationary time. Let's define the number of wash-outs as $N_w = \langle U \rangle T_{ss}/l_x$, which is the number of times an independent liquid volume injected into the domain travels along the entire streamwise direction. Previous works in Salvador et al. (2018) demonstrated that for a total of $N_w \approx 4$ the turbulence statistics did not converge. In this study, to ensure statistics convergence, the transient part of the simulation (hence $t < T_t$) has been removed from the dataset, whereupon only the statistical stationary part was analyzed, having data output at each time step for a total of $N_w = 10$.

| $dx$ | $dt$ | $l_x$ | $l_{y,z}$ | $T_t$ | $T_{ss}$ |
|---|---|---|---|---|---|
| 2.34 | 4.0 | 2.4 | 1.2 | 0.04 | 0.26 |
| $\mu m$ | $ns$ | $mm$ | $mm$ | $ms$ | $ms$ |

Table 2: Simulation setups.

### *2.3. The pseudo-fluid approach*

Most DNS studies in literature, relies on a priori knowledge (or determination) of the Kolmogorov scale, defined as $\eta = (\nu^3/\epsilon)^{1/4}$, where the energy dissipation rate is $\epsilon = 2\nu\langle s_{ij} s_{ij} \rangle$, being $s_{ij} = (\partial_j u_i + \partial_i u_j)/2$ the strain rate tensor. For a number of reasons, determining $\eta$ in multiphase flows is non trivial and atomizing liquid jets present even more challenges.

In a first place, $\nu$ cannot be defined as in single phase flows, due to the mixing induced by turbulence. This issue has been addressed in many works Gréa et al. (2014); Lee et al. (2008); Gauding et al. (2018) for single phase flows composed of fluids with different viscosities. In these studies, where the diffusion term is added in Equation (3), the authors proved that the hypothesis made by Taylor (1935) (stating that the normalized average dissipation is independent of the viscosity). In other words, the energy dissipation equation becomes:

$$\epsilon = 2\langle \nu s_{ij} s_{ij} \rangle = 2\langle \nu' s_{ij} s_{ij} \rangle + 2\langle \nu \rangle \langle s_{ij} s_{ij} \rangle = \epsilon_{\nu'} + \epsilon_{\langle \nu \rangle} \tag{4}$$

where the fluid viscosity has been decomposed into its average and pulsating components (namely $\langle \nu \rangle$ and $\nu'$). In round atomizing liquid jets, despite the presence of an interface, the flow is expected to behave in a statistical similar fashion, as the velocity derivatives would compensate the variation of viscosity Gauding et al. (2018). Furthermore, if the region is diluted enough, a number of droplet with significant kinetic energy will populate the domain, but ultimately, the predominant phase is expected to be the gaseous one, hence $\epsilon \approx 2\langle \nu \rangle \langle s_{ij} s_{ij} \rangle$ is a legitimate approximation. This hypothesis is especially valid within the disperse region and its accuracy will improve along the radial distance, further from the spray axis.

Once the energy dissipation rate is defined, the Kolmogorov scale can be uniquely defined in a consistent way, as:

$$\eta = \left(\frac{\nu^3}{\epsilon}\right)^{1/4} = \left(\frac{\langle\nu\rangle^3}{2\langle\nu\rangle\langle s_{ij}s_{ij}\rangle}\right)^{1/4} \tag{5}$$

Another reason for approaching the definition of $\epsilon$ in such a way, lies in the experimental studies of this phenomena. While the first formulation in Equation (4) can be used in DNS, it is implicitly simpler to estimate a mass concentration (hence a average viscosity) in experiments Desantes et al. (2011).

What discussed above is clearly a pseudo-fluid method, where the complexity of atomization is simplified by a averaged-properties fluid. It is important to convey that the term "pseudo-fluid" is adopted in order to establish a clear understanding of the approach used rather than a significant new synthetic field. In fact, this approach merely requires to use the average volume concentration for describing the local averaged properties, as according to Equation (2), where $C$ is substituted by $\langle C\rangle$. While implications on the flow analysis will be discussed later in Section 3 (with a specific effort on the repercussions of Equation (4)), here a discussion of the main reason behind the adoption of this approach is required. The discontinuity of properties through the interface and the dispersed nature of the flow are limiting factors in providing an accurate description of the flow properties, when scales need to be defined. For example, lets take into account Equation (5), where the time averaged viscosity is used. In a strongly anisotropic, non periodic flows, such as sprays are, applying the knowledge of the Kolmogorov scale as the smallest scale in the flow limits quite significantly the amount of information that could be extracted from this parameter. In fact, it may also be of interest to understand how fast turbulence is decaying as we move in the radial direction, away from the spray centerline, reducing its capability of mixing with the quiescent air. In this case, defining the flow properties through a pseudo-fluid approach offers an immediate understanding of the value of the Kolmogorov scale as the smallest kinematic motion scale occurring in correspondence with the specific local mixing levels. It is therefore useful to describe the fluid as a specific mixture, characterized by the local value of $\langle C\rangle$. As it will be discussed later in Section 3.4, the approach also allows for interesting comparison with single phase flows turbulence data.

Another very important aspect that should be considered for a correct understanding of this approach is the region where the method is applied. In this work, this approach is applied only to the disperse region, as is the region where the stronger atomized field (e.g. virtually all the liquid in this region is not connected with the liquid within the nozzle). In this region, the average volume fraction (i.e. $\langle C\rangle$) is expected to decreased significantly even in the spray centerline.

### *2.4. Spectra and similarity with gaseous jets*

The amount of data generated by a DNS simulation may be overwhelming and its processing represents a serious challenge. Additionally, data required for spectral studies need to be sampled at a high frequency and for a statistically significant time (that needs to be significantly larger than the integral time). These factors led to the development of the methodology used in this work. As the theory of jets Pope (2001), their statistical behavior Hussein et al. (1994) and their spectral behavior Antonia et al. (1986); Schmidt et al. (2018) have been widely characterized along the years, it is convenient to extend this common knowledge to two-phase sprays, due to the apparent similarities between the two cases Lefèbvre et al. (1989). In fact, both flows have a significant anisotropy in the axial direction: the mean axial velocity component is responsible for the generation of the highest contribution to the turbulent energy, whereas the turbulent kinetic energy associated with the radial and the azimuthal components contributes to the spreading of the spray, leading to the notorious cone angle. Measurements in the self-similar region show that the statistical behavior of the fluid evolves differently in the radial direction, but develops a statistical stationarity along the azimuthal direction. In other words, by changing the azimuthal coordinate, while fixing the radial position and the spray axial position, it is possible to represent both the first and second order statistical moments as functions of the sole radial position.

For this reason, it seems legitimate to assume that, over a sufficiently long time, also the frequencies typical of the flow should exhibit a similar behavior, presenting a consistent distribution of energy content over wavelengths as a function of the radial position. As a consequence, only a part of the simulation domain

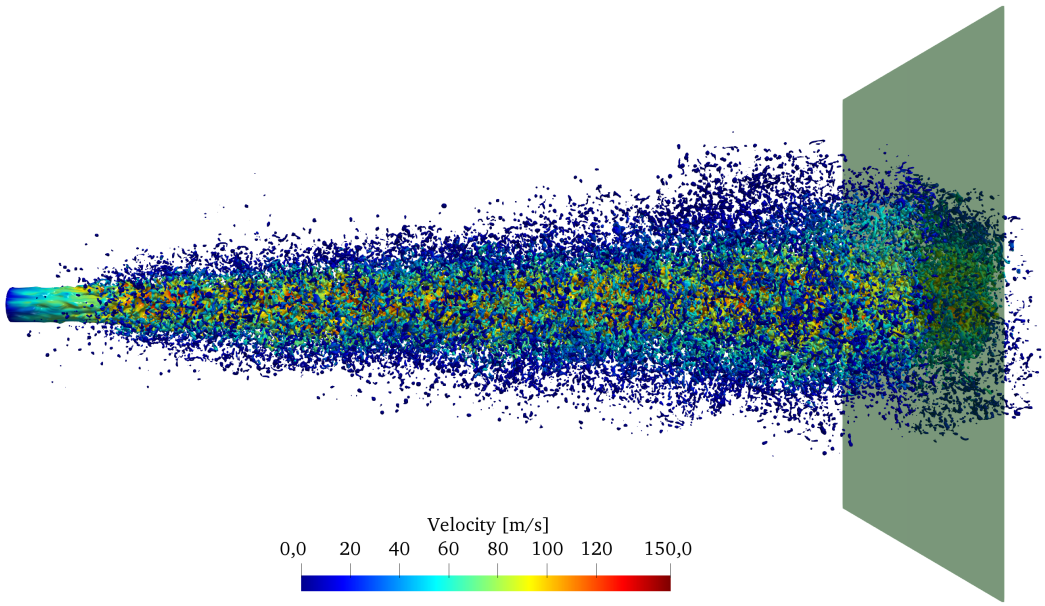


Figure 1: Render of the simulation at $t = T_t$. The green sub-domain represents the actual space region over which the spectral analysis of the flow was conducted. The contour for $C = 0.3$ is here colored using the flow velocity field.

was analyzed with a high time resolution in order to optimize the data analysis during the simulation post-process. Figure 1 shows a simulation render with a shadowed green region representing the sub-domain selected for the spectral analysis, where the iso-contour for $C = 0.3$ has been colored according to its velocity. This region, located at $x/D \approx 25$, reaches to the whole radial distance (i.e. $l_y$ and $l_z$), an axial length of 4.68 $\mu m$ and it is output at each time step for $T_t < t < T_{tot}$.

The statistical stationarity of the flow along the azimuthal coordinate combined with the pseudo-fluid approach offers also an interesting opportunity for computing the flow spectra. In fact, this combination allows to consider each radial position (i.e. each point at a certain radial distance along the azimuthal coordinate) as composed by the same pseudo-fluid composition, hence allowing consistency with the Taylor hypothesis. Therefore, analyzing the flow spectral behavior along the azimuthal direction would neglect possible contributions introduced by the different pseudo-fluid composition along the radial position, which effects may be difficult to separate and understand. For what discussed above in Section 2.3, fixing a radial distance where the pseudo-fluid composition is fixed implies that the velocity fluctuations are consistently describing the same turbulent behavior.

Figure 2 shows the average axial velocity field, computed over $T_{ss}$. The blue lines represents the directions over which the analysis of the spectra is computed using an angular fixed distance of $\delta\theta = \pi/180$. The autocorrelation is then computed as:

$$R_{ij}(\xi) = \sum_{n=0}^{N_\theta - 1} u_i(d + \Delta\theta) u_j(\Delta\theta) \tag{6}$$

where $N_\theta = 360$ and $\xi$ is the dimensionless distance vector that goes from 0 to 1, in order to allow comparability between the autocorrelation functions computed at different radial positions. In Equation (6), $u$ stands for the pulsating velocity. A useful way to compare autocorrelation functions, that will be used in

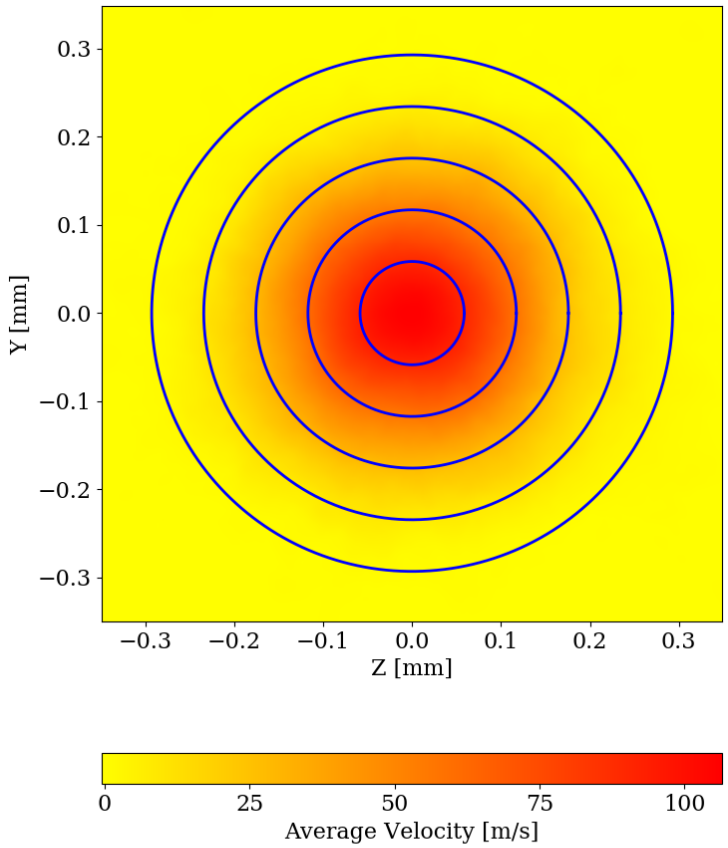


Figure 2: Average velocity field for the sub-domain analyzed in this work. The blue circles are the directions over which the autocorrelation and the spectra are computed.

this work, is by dividing for $\langle u(r,\theta,t)^2 \rangle$, as:

$$f_{11}(r,\delta\theta,t) = \frac{\langle u(r,\theta,t)u(r,\theta+\delta\theta,t)\rangle}{\langle u(r,\theta,t)^2\rangle} \tag{7}$$

The energy spectra can then be computed as:

$$E_ij(\kappa_1) = \frac{1}{\pi}\int_0^\infty R_{ij}(\xi)e^{-i\kappa_1\xi}d\xi \tag{8}$$

where $\kappa_1$ is the wavelength and $\xi$ has to be used as a dimensional quantity. Finally, the results for the one-point statistics will be showed as a function of the radial position $r/r_{1/2}$, where $r_{1/2}$ is the radial position where the velocity has decayed by 50% with respect to its value over the spray centerline.

### *2.5. Inflow boundary condition*

While in previous works Salvador et al. (2018), a significant emphasis was given over the effect of boundary conditions, in this work, the main focus is the turbulent field generated within the flow in the atomized region. For this reason, a Large Eddy Simulation of a periodic pipe was performed in order to generate a physical nozzle turbulent flow that would increase the atomization level. Once the simulation has reached a statistical stationary state, a central plane was extracted every $\Delta t = 0.1\ \mu s$ with a linear interpolation of the velocity field.

## 3. Results

In this section, the main results of this work will be discussed. In a first place, the convergence of the statistics used in this work will be analyzed, highlighting the necessity of a significant number of wash-outs and of the usage of the statistical similarity in the azimuthal direction. Consequently, the implications of the pseudo-fluid approach will be discussed in detail, by providing a clear explanation of its effects on the energy dissipation rate. Finally, the spectral analysis of the flow will be presented, after a brief discussion of the autocorrelation functions obtained.

### *3.1. Statistics convergence*

As discussed previously, convergence of time-averaged variables are not per se a proof of convergence of a statistical stationary process like turbulence is. In fact, the authors in Salvador et al. (2018) show a self-similar velocity profile which almost reached statistical convergence, although the total average-time was about 3 washouts. The reason may be that the average performed here is not only temporal, but also spatial. Round sprays and jets have the common attribute of being axisymmetric, hence, statistically speaking many points at various azimuthal position and same radial position can be used to produce a smoother average. This procedure is robust from a physical standpoint, being widely used in turbulence analysis of jets Schmidt et al. (2018), while allowing to reduce the amount of data required to perform studies of turbulence.

Figure 3 shows the convergence for the probability function $\mathcal{P}(u)$ of the axial velocity pulsating component, $u$, at a radial position $r = 0.8r_{1/2}$. This radial position has been chosen as far enough from the spray center. In this region, still significant breakup (secondary mostly) is occurring and the turbulent structures are, as will be discussed later, generally significantly smaller than the radius. Furthermore, each series (except for the "one point's" one, that will be discussed later) have been computed by accounting for all the signals at all azimuthal positions, hence improving the statistical dataset. The series of $N_w = 10$ is the one used in general for all the statistics provided in this study. It is evident how the convergence is reached quite rapidly and already for $N_w = 1.7$ the results are quite similar. The higher the number of washouts $N_w$, the smoother the statistics result. The Cartesian mesh that the simulation provides, is interpolated into a cylindrical mesh of 90 radial positions and 360 azimuthal positions. In a first place, Figure 3 shows that velocity may have fluctuations that are comparable to the velocity average itself (that in this radial position may be around 60 $m/s$). This occurrences are captured even for low $N_w$, meaning that the phenomena has a significant statistical influence. On the other hand, the pseudo-Gaussian behavior of $\partial_x u$ decrease quite

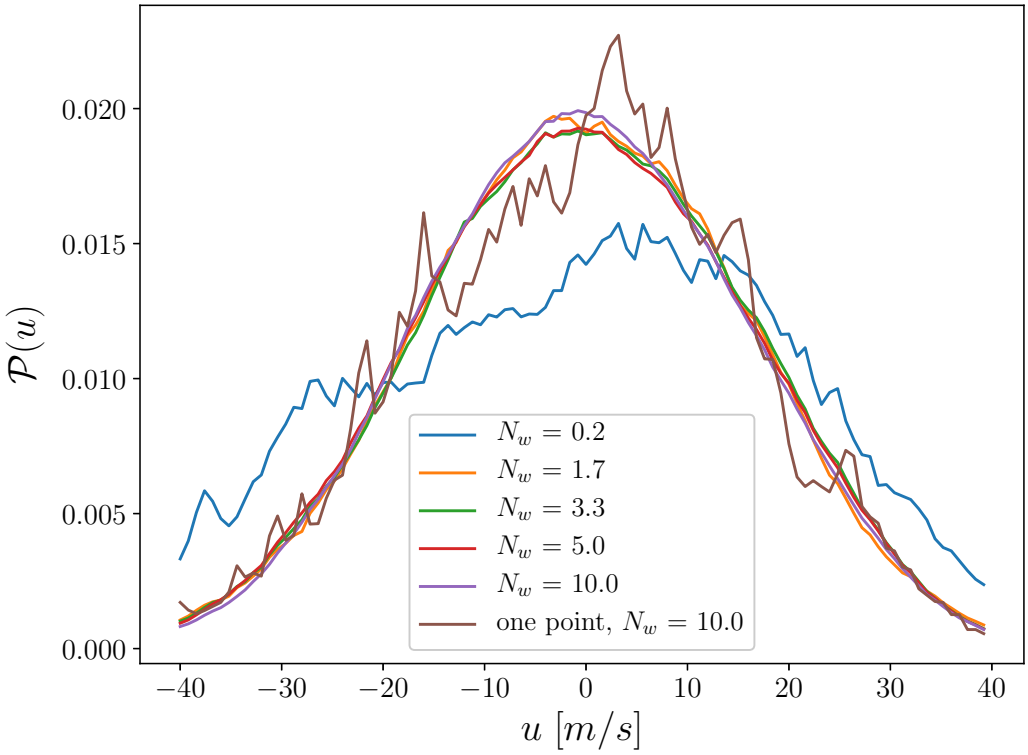


Figure 3: Convergence of probability function for the axial velocity pulsating component.

rapidly from its average peak, showing how turbulent structures are mostly transported axially and that their oscillations are quite small, as justified by the reduced turbulent field imposed by the low Reynolds number.

Another interesting dataset is the "one point", presenting the probability function of a single point, averaged over $N_w = 10$. It is immediately clear that the usage of a single point is not sufficient for obtaining a smooth probability function even for $N_w = 10$. On the other hand, the usage of all the points over the azimuthal coordinate is a clear indicator that statistically similar regions can be used to achieve smoother probability distributions. Once again, this results further strengthen the parallelism between the atomizing round sprays and the round gaseous jets.

### *3.2. The pseudo-fluid one-point statistics*

As extensively described in literature Pope (2001); Frisch (1995), the classic theory of turbulence relies heavily on the description of the fluid properties. While in single phase flows these are easy to assess (in lack of compressibility or thermal gradients), in multiphase flows the issue is more substantial, throwing shades over the reliability and applicability of single phase turbulence in multiphase flows Duret et al. (2011); Ling et al. (2019). In fact, as a significant limit for the smallest scales of motion is imposed by the interface thickness, it is arguable that viscosity is still the only mechanism of dissipation Desjardins and Pitsch (2010).

The choice of using a pseudo-fluid approach is actually a way to address the multiphase turbulence and simplify an extremely complex scenario. In fact, the instantaneous description of the flow relies on its local properties $\rho(\mathbf{x}, t)$ and $\nu(\mathbf{x}, t)$, which are both function of time and position. The pseudo-fluid assumption in this case translates into accounting the time-dependence of these properties by substituting them by their time-average value in time. This may have some serious consequences in the determination of one-point

statistics. In order to compute the average viscosity $\langle\nu\rangle$, the time-average volume fraction $\langle C\rangle$ is used and it is showed in Figure 4, from which a series of considerations can be drawn. In a first place, the value in the centerline is $\langle C\rangle \approx 0.23$, which justify the assumption of a quite dilute zone. The steepness of $\langle C\rangle$ for $r < r_{1/2}$ also provides informations about the fact that the main direction of advection in this region is still the axial one (otherwise the droplet advected radially would have decreased the curve steepness). The results in Figure 4 can be used instead of the Heaviside function in Equation (2) to compute the time-average viscosity. It should be noted that the original density ratio $\rho_l/\rho_g \approx 32$ and the viscosity ratio $\nu_l/\nu_g \approx 2.2$ are reduced significantly by the results in Figure 4 in this region.

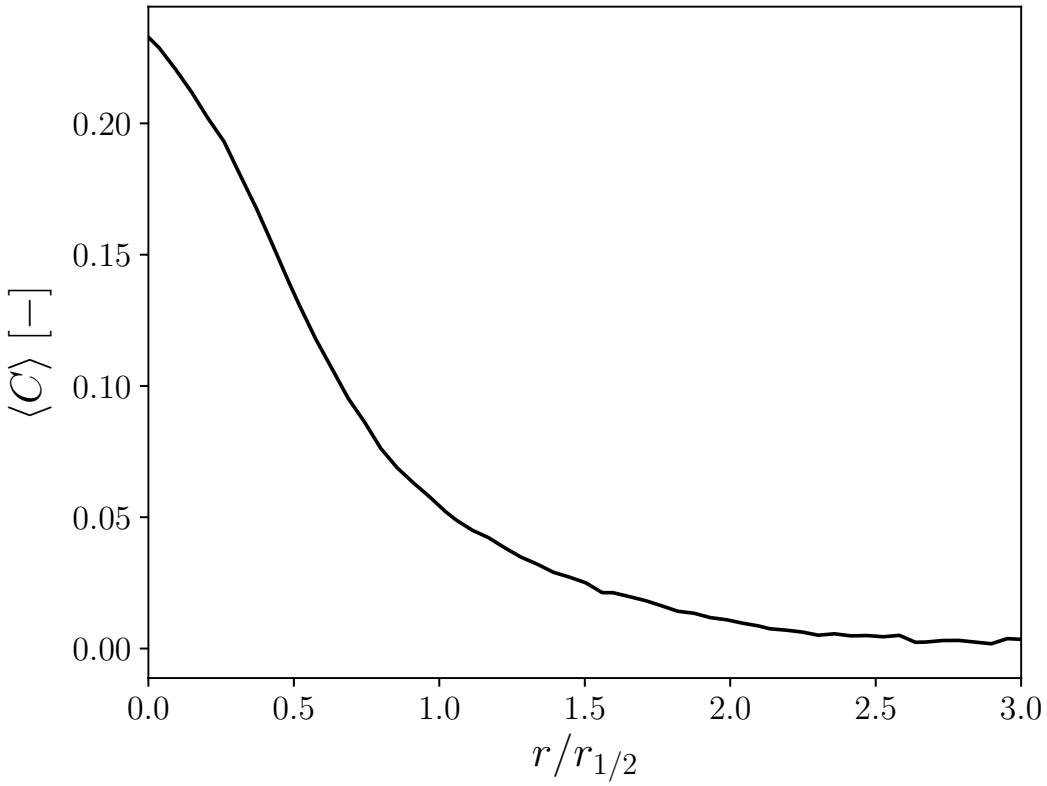


Figure 4: Time-average volume fraction as a function of the radial position.

The result of the pseudo-fluid approximation is showed in 5, where all the terms in 4 are showed. As emerges from the analysis, the term $\langle\nu' s_{ij} s_{ij}\rangle$ is negligible in respect to the average term $\langle\nu\rangle\langle s_{ij} s_{ij}\rangle$, suggesting the validity of the pseudo-fluid approach. Similar results have been found for variable viscosity fluid mixtures by Gauding et al. (2018), where the fluctuating term also was negligible for small viscosity ratios, despite the significant different fashion with which mixing occurs in miscible fluids instead of multiphase flows.

Although the error is mostly negligible (i.e. small $\langle\nu' s_{ij} s_{ij}\rangle$), some further considerations can be made in the region where the error is most significant ($r/r_{1/2} < 1$). In order to further understand why this region is particularly subjected to larger errors, both the changes in the pseudo-fluid composition and the turbulence level in this region may be analyzed. Once again, using the pseudo-fluid approach (i.e. the results obtained in Figures 4 and 5) can be used to calculate the Taylor scale based Reynolds number as :

$$Re_\lambda = \frac{\sqrt{\langle u'^2\rangle}\lambda}{\nu} \tag{9}$$

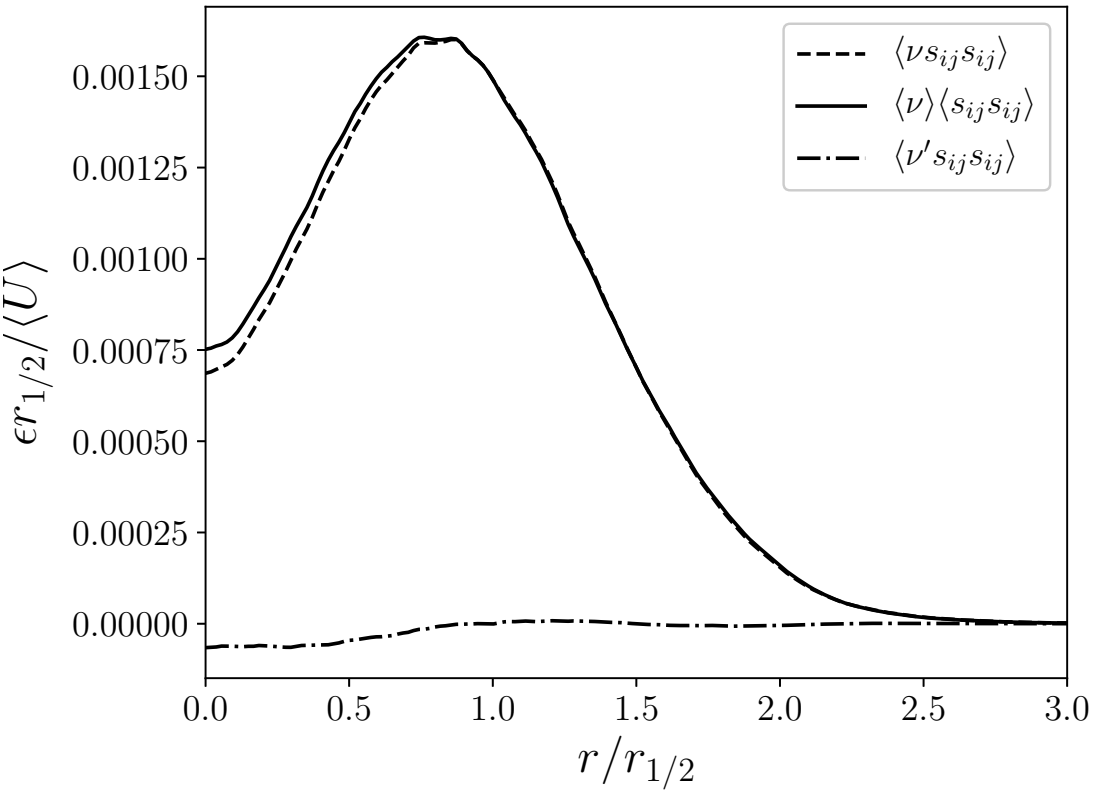


Figure 5: Average energy dissipation terms, as presented in Equation (4).The contribution of each terms are represented against their radial position. The values are made dimensionless by using $r_{1/2}$ and the average injection velocity $\langle U \rangle$

where $\langle u'^2 \rangle$ is referring to the average of the summed square of each velocity component and $\lambda$ is defined as the Taylor microscale from Taylor (1935):

$$\lambda = \sqrt{\frac{15\nu \langle u'^2 \rangle}{\epsilon}} \tag{10}$$

The results for $Re_\lambda$ are displayed in Figure 6. The comparison between Figures 5 and 6 shows a very similar behavior as expected. The error in Figure 5 between $\langle \nu s_{ij} s_{ij} \rangle$ and $\langle \nu \rangle \langle s_{ij} s_{ij} \rangle$ is maximum for $r = 0$ and decreases until $r \approx r_{1/2}$. This region is within the mixing layer and it justify the larger error given by the effect of $\nu'$. For $r > r_{1/2}$ the mixing is already significantly smaller, with $\langle C \rangle|_{r=r_{1/2}} < 0.25 \langle C \rangle|_{r=0}$, meaning that the actual probability of finding droplets (hence liquid surface) in this region is significantly reduced with respect to the spray axis. This considerations leads to one of the possible limitations of this approach, i.e. a significant increment of the estimation error in denser regions. On the other hand, it is also important to keep in mind the different effects on the error of $\langle C \rangle$ and $\partial_t \langle C \rangle$. In the very proximity of the nozzle, the liquid and gas regions are well defined (e.g. results displayed in Figure 1), hence $\langle C \rangle$ transition between the two phases is pretty sharp, while $\partial_t \langle C \rangle$ is practically null except for the interface on the external intact core length. Similarly, in intermediate regions, the value of $\langle C \rangle|_{r=0}$ is higher than the one observed on the centerline of the subdomain analyzed here, while the derivative $\partial_t \langle C \rangle$ is likely still lower due to less atomization occurring in this region. As discussed above, even in regions where atomization is pretty dominant like the one observed here, the error associated with the term $\nu'$ (strictly related to $\partial_t \langle C \rangle$) is negligible, allowing for legitimately testing this approach in other flow regions. In the authors opinion, due to the very small inaccuracy displayed in Figure 5, the error in denser regions is likely to be still negligible

also because of the small viscosity ratio displayed by the liquid-gas combination. It is also important to remark that this flow combination (being nitrogen and n-dodecane at ambient conditions) is extremely representative of fluids used in typical applications where atomizers are employed. These assumptions need a more wide scientific proof and further future studies.

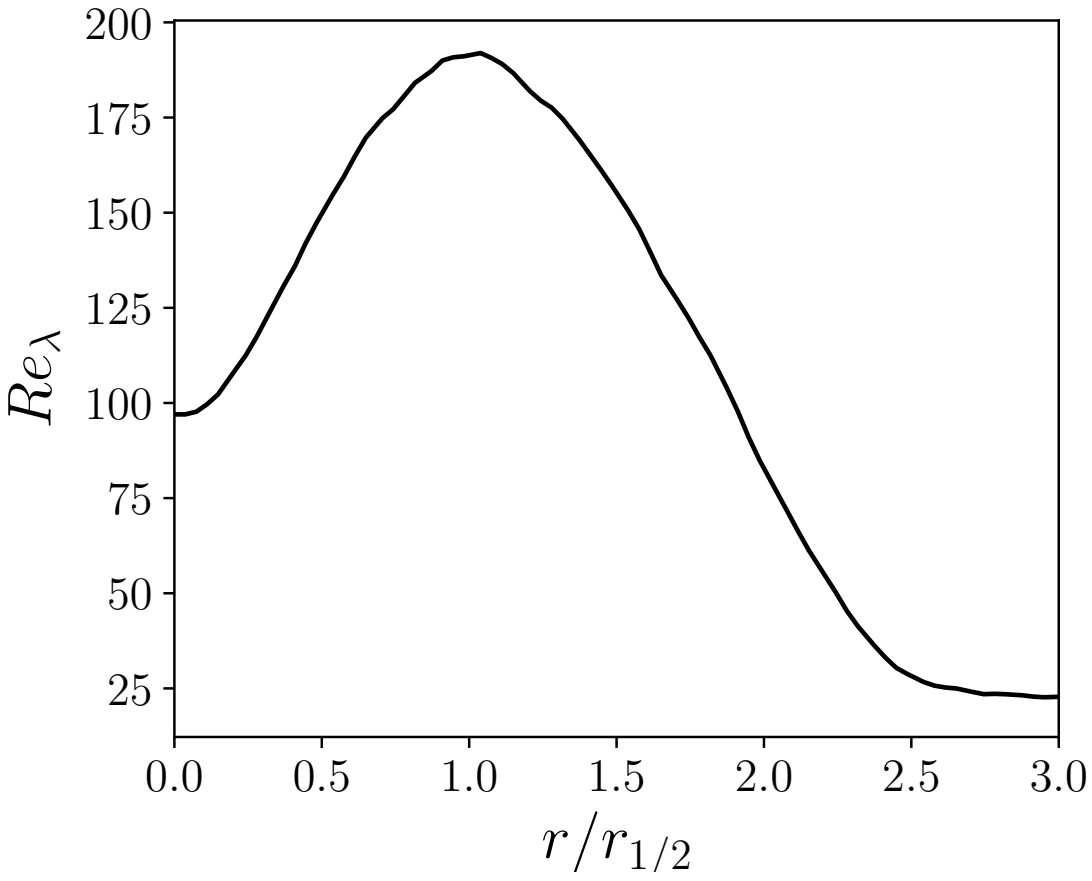


Figure 6: $Re_\lambda$ as a function of the radial position.

An interesting consideration emerges from this analysis. Although the interface is a key factor in creating turbulence (e.g. via Kelvin-Helmholtz instability and droplet dispersion), its effect on the average analysis of turbulence is most likely a second order effect in primary atomization. This may be a strong statement and needs further study and validation, although, if proven, could affect significantly the future studies of turbulence in multiphase flows. In fact, this hypothesis could also be a significant way to simplify the sub-grid modeling of turbulence in multiphase flows. Furthermore, unlike studies with droplets within HIT, primary atomization displays a significant range of droplets diameter at various locations, hence removing any possible correlation given by both droplets' spacing (distance between each droplet), velocity and diameter with the flow's turbulence statistics. Finally, it is important to remark that the pseudo-fluid approach should not be considered as a method to neglect the interface effects. In case of Figure 5 it appears quite evidently that the terms involving the fluctuating viscous term is quite negligible, hence, the dissipation associated with the interface dissipate less energy than the velocity fluctuations tipical of the turbulent field.

Accordingly to what discussed above, also the Kolmogorov scale can be computed and the result is showed in Figure 7. The Kolmogorov scale actually provides a very interesting insight on the flow behavior. In a first place, unlike the calculation of the Kolmogorov scale in particle-laden Park et al. (2017); Bassenne et al. (2019) and droplet in isotropic turbulence Elghobashi (2018), here the flow is strongly anisotropic,

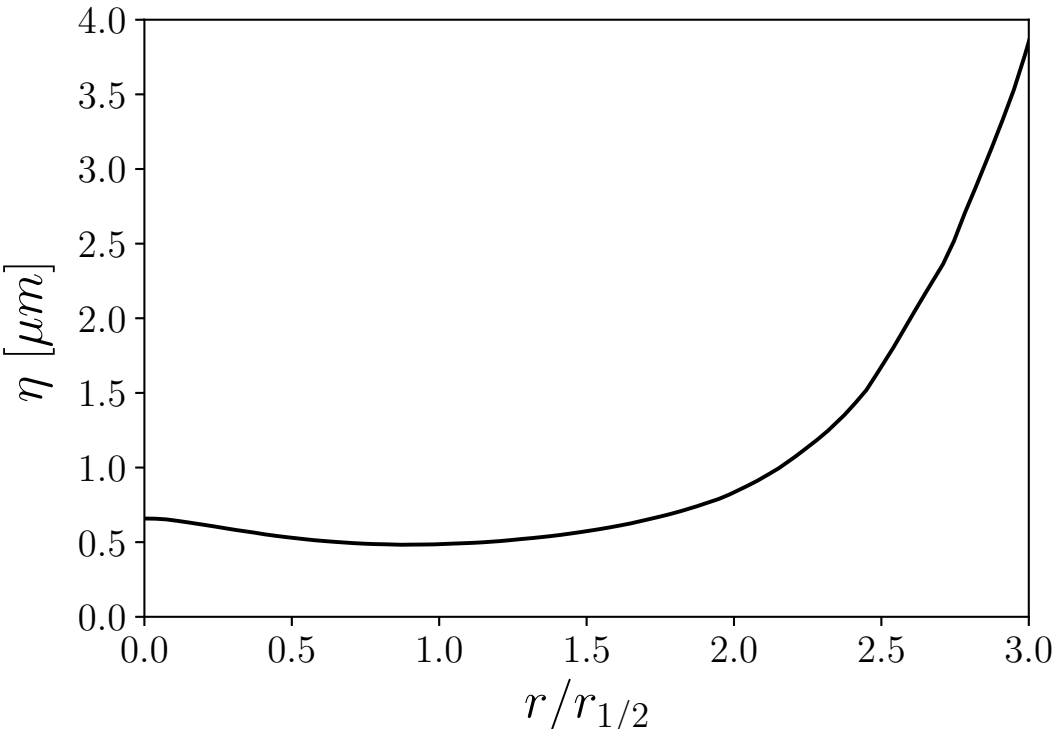


Figure 7: Kolmogorov scale as a function of the radial position.

hence the local value of the Kolmogorov scale changes with the radial position. While this statement seem in contradiction with the academic explanation of this scale (usually described as the lengthscale characterizing the smallest eddies in a flow, hence uniquely defined by a single value) it actually opens up a newer interpretation of the scale in such a context. The smallest eddies are also characterized by a short timescale, hence they dissipate quite rapidly. It is therefore assumable that while they may get advected axially by the main flow, their radial displacement may be too slow to actually transmit the eddies generated in higher turbulent region to the outer diameters. If that is the case, the information condensated in Figure 7 may be an excellent guideline for reducing the computational time required for these flows' simulation. In fact, as the mesh size may decrease rapidly with the radial position, the information over $\eta$ may provide a useful guideline for algorithms like AMR, in order not to lose sensible information over the turbulent structures.

It is once again important to consider the implications of the pseudo-fluid approach in the understanding of the Kolmogorov scale. We already pointed out that using this assumption allows to consider this scale as the smallest motion scale occurring is a region characterized by a specific mixing and mixture, quantifiable by $\langle C \rangle$ but it is important also to underline that in multiphase flows, this scale does not represent anymore the overall smallest scale, as interface phenomena are likely to occur on a far smallest scale. On the other hand, using this approach will allow in the next sections to compute interesting quantities, such as scale separation and dimensionless spectra. Therefore, it is clear that the pseudo-fluid approach represents mostly an interesting tool to use turbulent theoretical concepts, typical of single phase flows, in context such as sprays or, more in general, multiphase flows, finally allowing possible parallel analysis between the two. For example, results from DNS simulations could be used to improve sub-grid models of Large Eddie Simulations by accounting for different spectrum dissipation tail (high $\kappa$), corresponding to local levels of average volume fractions. Finally, the proof of the reduced error linked to the fluctuating component of the viscosity $\langle \nu' \rangle$ in Figure 5 may be extremely handy in conditions where measuring both the velocity fluctuation and the fluid composition may be challenging (e.g. experiments).

### 3.3. Autocorrelation and integral lengthscale

The first step in analyzing the flow spectra is computing the autocorrelation function, as discussed in Section 2. Also just in itself, the autocorrelation gives an estimation on whether a turbulent structure can be defined within a certain length, hence it is interesting to analyze it in order to understand the implications of the method used. For example, an autocorrelation that does not reaches zero is symptomatic of a turbulent structure that cannot be entirely defined within the length considered. Due to the radial approach that has been used in this work for the spectral analysis, the autocorrelation at low radial distance from the spray centerline have a limited perimeter, hence they are likely to not reach zero, as some larger structures that goes through the spray centerline are indeed larger than the relative perimeter. This side-effects rapidly mitigates as the radial position increase and soon becomes secondary.

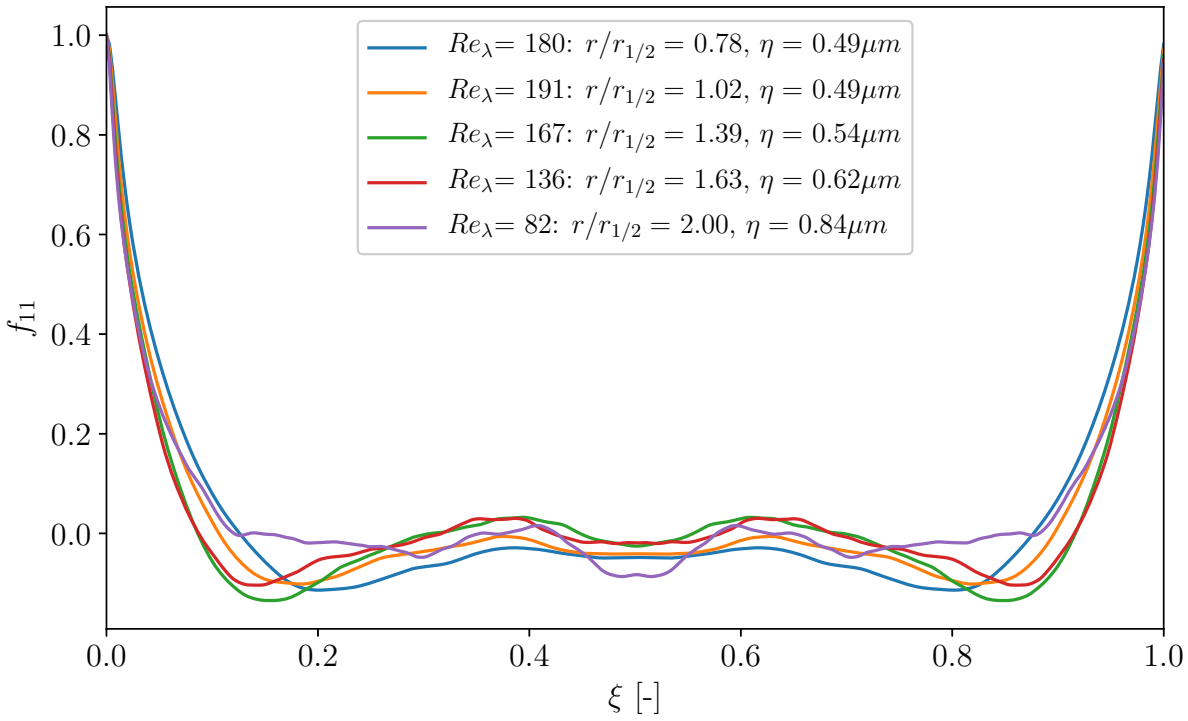


Figure 8: Autocorrelation function $f_{11}$ as a function of the dimensionless azimuthal coordinate $\xi$. In the legend each curve is described by its radial position ($r/r_{1/2}$), its Reynolds-Taylor number ($Re_\lambda$) and its Kolmogorov scale $\eta$.

Figure 8 shows the autocorrelation function $f_{11}$ (described in Equation (7)) as a function of the dimensionless azimuthal coordinate $\xi$. In the legend each curve is described by its radial position ($r/r_{1/2}$), its Reynolds-Taylor $Re_\lambda$ number and its Kolmogorov scale $\eta$. The radial positions showed have been picked to avoid the above mentioned effect (where the autocorrelation does not reach zero). All the autocorrelation picked show a rapid decay, meaning that the turbulent structures have a characteristic size that is significantly smaller than the radial perimeter over which the autocorrelation is computed. Also, the farther from the spray axis, the more rapidly the autocorrelation decays and this behavior can be explained by the fact that, as stated above, the perimeter over which the $f_{11}$ is computed increase with the radius.

Another interesting consideration can be made by computing the integral lengthscale $L_{11}$ as:

$$L_{11} = \int_0^{2\pi} f_{11}(r, \theta) d\theta \tag{11}$$

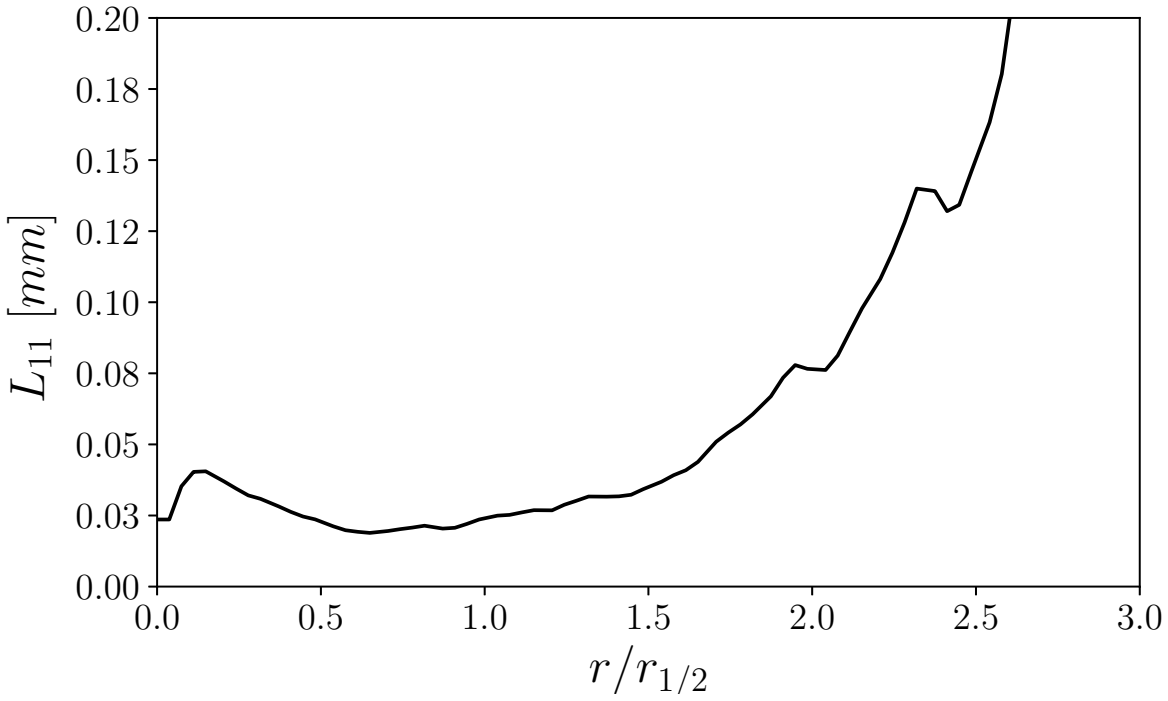


Figure 9: Integral lengthscale $L_{11}$ as a function of the dimensionless radial position ($r/r_{1/2}$).

The result, as a function of the dimensionless radial position ($r/r_{1/2}$) is showed in Figure 9. The overall behavior is quite similar to the Kolmogorov scale in Figure 7, showing a scale separation ($L_{11}/\eta$) within $1-2$ orders of magnitude. Again, the information regarding the region close to the spray centerline should be taken with criticism, as the autocorrelation in that area is evaluated over a perimeter which is likely smaller than the structures related to the axial pulsating velocity in that region. It can be noted that, within the mixing region, the integral lengthscale is of the order of the nozzle radius, while progress quite rapidly to almost twice the diameter as the radius increases. This information also provides a interesting insight on how the Kolmogorov scale is computed in order to justify, a priori, the mesh size in DNS simulations. In fact, in many works Lebas et al. (2009); Gorokhovski and Herrmann (2008); Hasslberger et al. (2019) the determination of the Kolmogorov scale (hence the mesh size) relies on the parameters provided for the turbulence developed within the nozzle flow (e.g. the turbulent lengthscale $L$ and the turbulence intensity $I$ in Salvador et al. (2018)). The difference between this value of $L_{11}$ and the one found analyzing the LES simulation used to extract the boundary condition (i.e. $L = 0.058D$ in this study) shows clearly why this practice should not be, in the author opinion, pursued. On the other hand, this approach is reasonable in lack of data to compute $\eta$ otherwise.

### *3.4. Kolmogorov spectra scaling*

Using the autocorrelation data (in their dimensional form) showed in Figure 8, the one dimensional energy spectra of the flow can be computed. Figure 10 shows the energy spectra, made dimensionless using the Kolmogorov scaling Pope (2001); Saddoughi et al. (1994). Each value of $\eta$, $\nu$ and $\epsilon$ has been taken at the exact radial position where the respective autocorrelation is computed from the data displayed in previous section in this paper. The Kolmogorov scaling representation of the one-dimensional spectra presents many advantages. In a first place, it enables the comparison of different spectra computed in various ways, from both experimental and numerical analysis. In Figure 10, the comparison with data from Uberoi and Freymuth (1970); Saddoughi et al. (1994); Harris et al. (1977); Comte-Bellot and Corrsin (1971) (as reported in Pope (2001); Saddoughi et al. (1994)) is showed. The spectra for different radius collapse

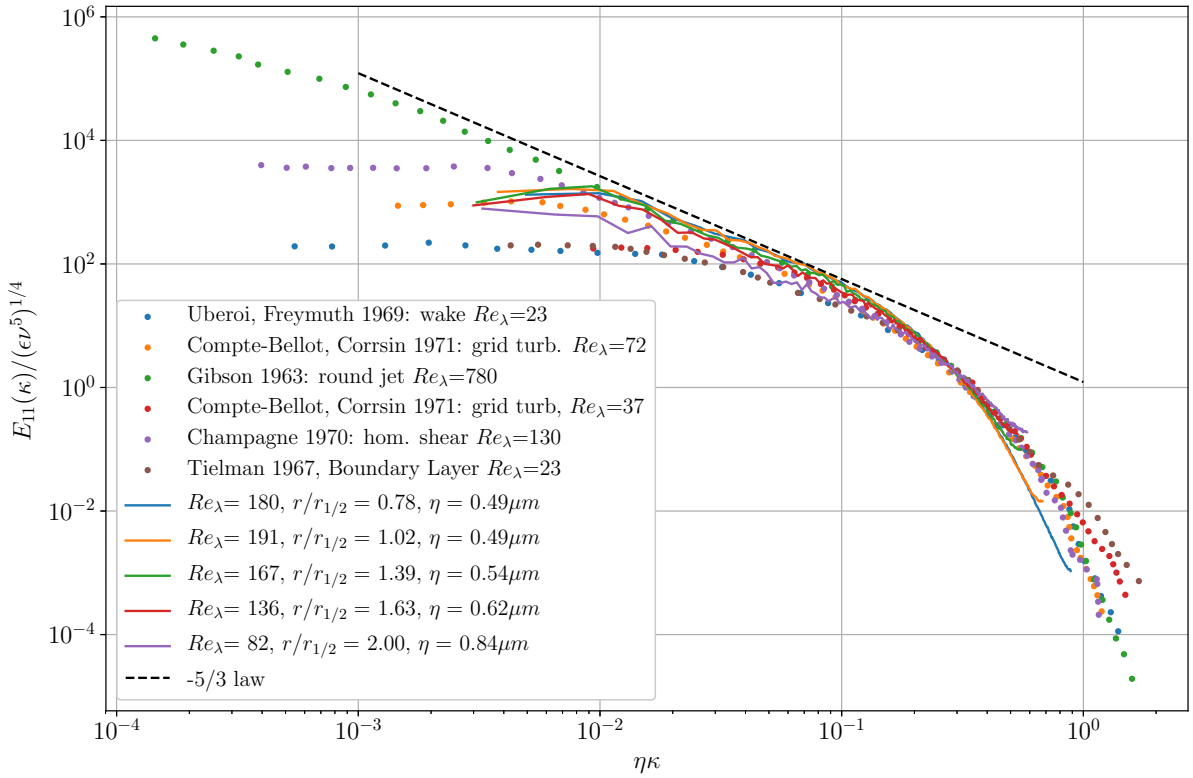


Figure 10: One dimensional energy spectra showed using the Kolmogorov scaling. Continuous lines are the results obtained for the simulation in this work at different radial positions, while dotted lines are literature data. For the continuous lines, each iso-radius spectra is made dimensionless using its respective Kolmogorov scale in Figure 7 and the respective $\epsilon$ (Figure 5) and $\nu$. The data are from Uberoi and Freymuth (1970); Saddoughi et al. (1994); Harris et al. (1977); Comte-Bellot and Corrsin (1971).

for $\kappa\eta \approx 0.1$ as discussed in Pope (2001). This behavior is typical of flows that verify the first similarity hypothesis of Komogorov's turbulence theory, for which it can be proved (see Pope (2001); Frisch (1995)) that the one dimensional spectra is a function of $\kappa\eta$ in such region.

Thanks to the Kolmogorov scaling, some interesting considerations over the pseudo-fluid approach can be made. In fact, the curve collapsing shows that the turbulence behavior, although changes significantly with the radial position, maintains a behavior coherent with the Kolmogorov first similarity hypothesis. Furthermore, this also implies that the velocity spectra is not significantly affected by the atomization process. In fact, Figure 4 shows that for $0 \leq r/r_{1/2} \leq 2$ there is still a quite significant atomization activity, therefore the droplet and breakup should affect the spectra. Instead, this data shows that it is likely that the breakup is actually a mechanism that interact the turbulence in a bi-directional way, therefore no significant disruption of the spectra in the transition between the inertial subrange and the dissipation range is caused, explaining the curves collapse for $\kappa\eta \approx 0.1$.

A few words are in order as this results is substantially in contrast with the ones observed in other multiphase flows, such as bubbly flows Roghair et al. (2011); Prakash et al. (2016) and particle/droplet-laden flows Dodd and Ferrante (2016); Lucci et al. (2010), while corroborating other spectral behaviors observed in primary atomization Ling et al. (2019); Agbaglah et al. (2017); Desjardins and Pitsch (2010). An interesting explanation for bubbly flows is provided in Prakash et al. (2016), where they discuss the coexistence of the -5/3 and -3 power-law scaling. In fact, while the pseudo-turbulence -3 power-law is generated by the bubble buoyancy Roghair et al. (2011), the -5/3 is generated by the grid-turbulence induced in the experiment. The spectra deviation occurs at frequencies tightly related with the bubbles typical wavelength given by

the diameter which is controlled in order to generate bubbles of predefined size. In droplet laden Dodd and Ferrante (2016), a similar disruption of the spectra is observed, although the reasoning of the authors of these works is substantially different Elghobashi (2018). In droplet-laden flows a deviation of the spectra is observed at a wavelength that can be related to the size of the droplets populating the domain at the beginning of the simulation and the spectra is flatter (i.e. the slope is higher than $-5/3$) as can be justified by the absence of any forcing term, such as the buoyancy in bubbly flows. Regardless of the different fashion with which the spectra behaves, the presence of a specific frequency where the spectra deviation can be detected is quite revealing. In fact, in primary atomization, many authors Ling et al. (2019); Agbaglah et al. (2017); Desjardins and Pitsch (2010) have observed almost exclusively -5/3 slopes, In our opinion, the reason for the lack of deviation of the spectra can be found in two fundamental observations. In a first place, the number and sizes of droplets changes significantly in primary atomization (see the discussion in Section 1), hence no specific frequency can be detected. In a second place, in the simulations of primary atomization mentioned here and in the present work, the turbulence and breakup events are not forced or artificially induced, rather are naturally generated by the injection of liquid at a high momentum from the nozzle and the Kelvin-Helmholtz instability, giving an entirely different context where evidences suggest that turbulence only display a -5/3 scaling. These observations will have to be further supported by future analysis and better explained in future works.

On the other hand, it is important to notice that while the comments above are valid regardless of the turbulence intensity displayed within the flow (as confirmed by the findings of Uberoi and Freymuth (1970)) this case shows a limited turbulence behavior, as the $-5/3$ law of the inertial subrange actually applies only for one order of magnitude on the wavelength axis, symptom of a reduce scale separation. Still, this context provides an excellent test-case to prove the method that has been used in analyzing the spray and provide a significant insight on the spray turbulent behavior.

## 4. Conclusion

The present work has presented an original methodology based on a pseudo-fluid method for describing the turbulence field within an atomizing liquid jet. The achievement of smooth statistics was possible in Section 3.1 thanks to both a temporal and a spatial average over a statistically similar direction, i.e. the azimuthal direction, similarly to the usual procedure in analyzing singlephase jets Schmidt et al. (2018). The combination of smooth statistics as well as the usage of the smooth properties field provided by the pseudo-fluid approach allowed to achieve a neat values for the one-point statistics presented in Section 3.2. Among these analysis, the Taylor-Reynolds number $Re_\tau$, the energy dissipation rate $\epsilon$ and the Kolmogorov scale $\eta$ have been shown as a function of the radial position. The autocorrelation function and the integral length scale, computed by integrating the former, are presented and discussed in Section 3.3. Finally from the autocorrelation function the flow spectra is obtained in Section 2.4, where a comparison with literature data for single phase flows spectrum is performed.

The work provides, in the authors opinion, two interesting contributions. On one hand, the definition of a clear methodology for computing the one/two-point statistics and respective spectra is provided. A specific focus is posed over the methodology used, namely the pseudo-fluid approach, as a interesting way to simplify the analysis of multiphase turbulence. In fact, provided an estimation of $\langle\nu\rangle$ is viable, this method can also be used for experimental analysis, without, in principle, lacking of significant accuracy. The main objective of future works will be the definition of a limit for the applicability of this method, defining up to which gradient and maximum value for $\langle C\rangle$ the method mainteins its accuracy.

Finally, this work provides the estimation of some fundamental values for designing DNS simulation of atomizing jets, as the Kolmogorov scale, the integral lengthscale and the Taylor-Reynolds number. These values, aside from providing a significant insight on the turbulent behavior of sprays, also allow to improve the design process of atomizing jets simulations. For example, the results for $\eta$ may be useful in controlling Adaptive Mesh Refining algorithms or, in general, estimating the amount of energy lost in under-resolved DNS simulations.

## Acknowledgements

This research has been partially funded by Spanish Ministerio de Economía y Competitividad through project RTI2018-099706-B-100, "Estudio de la atomizacion primaria mediante simulaciones DNS y técnicas ópticas de muy alta resolucion". Additionally, the authors thankfully acknowledge the computer resources at MareNostrum 4 (Barcelona Supercomputing Center) and their technical support provided by FI-2017-2-0035 and TITAN (Oak Ridge Leadership Computing Facility) in the frame of the project TUR124.

## References

Agbaglah, G., Chiodi, R., Desjardins, O., 2017. Numerical simulation of the initial destabilization of an air-blasted liquid layer. Journal of Fluid Mechanics 812, 1024–1038. doi:doi:10.1017/jfm.2016.835.

Aliseda, A., Hopfinger, E.J., Lasheras, J.C., Kremer, D.M., Berchielli, A., Connolly, E.K., 2008. Atomization of viscous and non-newtonian liquids by a coaxial, high-speed gas jet. Experiments and droplet size modeling. International Journal of Multiphase Flow 34, 161–175. doi:doi:10.1016/j.ijmultiphaseflow.2007.09.003.

Aniszewski, W., Zaleski, S., Llor, A., Malan, L., 2018. Numerical simulations of pore isolation and competition in idealized micro-spall process. International Journal of Multiphase Flow URL: https://linkinghub.elsevier.com/retrieve/pii/S0301932218303082, doi:doi:10.1016/j.ijmultiphaseflow.2018.10.013.

Antonia, R.A., Anselmet, F., Chambers, A.J., 1986. Assessment of local isotropy using measurements in a turbulent plane jet. Journal of Fluid Mechanics 163, 365. URL: http://www.journals.cambridge.org/abstract{_}S0022112086002331, doi:doi:10.1017/S0022112086002331.

Bassenne, M., Esmaily, M., Livescu, D., Moin, P., Urzay, J., 2019. A dynamic spectrally-enriched subgrid-scale model for preferential concentration in particle-laden turbulence. International Journal of Multiphase Flow URL: https://linkinghub.elsevier.com/retrieve/pii/S0301932218308231, doi:doi:10.1016/j.ijmultiphaseflow.2019.04.025.

Brändle de Motta, J.C., Costa, P., Derksen, J.J., Peng, C., Wang, L.P., Breugem, W.P., Estivalezes, J.L., Vincent, S., Climent, E., Fede, P., Barbaresco, P., Renon, N., 2019. Assessment of numerical methods for fully resolved simulations of particle-laden turbulent flows. Computers and Fluids 179, 1–14. doi:doi:10.1016/j.compfluid.2018.10.016.

Chorin, A.J., 1968. Numerical solution of the Navier-Stokes equations. Mathematics of Computation 22, 745–762. doi:doi:10.2307/2004575.

Comte-Bellot, G., Corrsin, S., 1971. Simple Eulerian time correlation of full-and narrow-band velocity signals in grid-generated, isotropic turbulence. Journal of Fluid Mechanics 48, 273–337. doi:doi:10.1017/s0022112071001599.

Desantes, J.M., Salvador, F.J., Lopez, J.J., De la Morena, J., 2011. Study of mass and momentum transfer in diesel sprays based on X-ray mass distribution measurements and on a theoretical derivation. Experiments in Fluids 50, 233–246. URL: http://link.springer.com/article/10.1007/s00348-010-0919-8, doi:doi:10.1007/s00348-010-0919-8.

Desjardins, O., Pitsch, H., 2010. Detailed Numerical Investigation of Turbulent Atomization of Liquid Jets. Atomization and Sprays 20, 311–336. doi:doi:10.1615/AtomizSpr.v20.i4.40.

Dodd, M.S., Ferrante, A., 2016. On the interaction of Taylor length scale size droplets and isotropic turbulence. Journal of Fluid Mechanics 806, 356–412. doi:doi:10.1017/jfm.2016.550.

Duret, B., Luret, G., Reveillon, J., Menard, T., Berlemont, A., Demoulin, F.X., 2011. DNS Analysis of turbulent mixing in two-phase flows. International Journal of Multiphase Flow 40, 93–105. URL: http://dx.doi.org/10.1016/j.ijmultiphaseflow.2011.11.014, doi:doi:10.1016/j.ijmultiphaseflow.2011.11.014.

Elghobashi, S., 2018. Direct Numerical Simulation of Turbulent Flows Laden with Droplets or Bubbles. Annual Review of Fluid Mechanics 51, 217–244. doi:doi:10.1146/annurev-fluid-010518-040401.

Frisch, U., 1995. Turbulence. Cambridge University Press. URL: https://www.cambridge.org/core/product/identifier/9781139170666/type/book, doi:doi:10.1017/CBO9781139170666.

Gauding, M., Danaila, L., Varea, E., 2018. One-point and two-point statistics of homogeneous isotropic decaying turbulence with variable viscosity. International Journal of Heat and Fluid Flow 72, 143–150. URL: https://doi.org/10.1016/j.ijheatfluidflow.2018.05.013, doi:doi:10.1016/j.ijheatfluidflow.2018.05.013.

Gorokhovski, M., Herrmann, M., 2008. Modeling Primary Atomization. Annual Review of Fluid Mechanics 40, 343–366. URL: http://www.annualreviews.org/doi/10.1146/annurev.fluid.40.111406.102200, doi:doi:10.1146/annurev.fluid.40.111406.102200.

Gréa, B.J., Griffond, J., Burlot, A., 2014. The effects of variable viscosity on the decay of homogeneous isotropic turbulence. Physics of Fluids 26. doi:doi:10.1063/1.4867893.

Harris, V.G., Graham, J.A.H., Corrsin, S., 1977. Further experiments in nearly homogeneous turbulent shear flow. Journal of Fluid Mechanics 81, 657–687. doi:doi:10.1017/s0022112077002286.

Hasslberger, J., Ketterl, S., Klein, M., Chakraborty, N., 2019. Flow topologies in primary atomization of liquid jets: A direct numerical simulation analysis. Journal of Fluid Mechanics 859, 819–838. doi:doi:10.1017/jfm.2018.845.

Hinze, J.O., 1955. Fundamentals of the hydrodynamic mechanism of splitting in dispersion processes. AIChE Journal 1, 289–295. doi:doi:10.1002/aic.690010303.

Hussein, H.J., Capp, S.P., George, W.K., 1994. Velocity measurements in a high-Reynolds-number, momentum-conserving, axisymmetric, turbulent jet. Journal of Fluid Mechanics 258, 31–75.

Kolmogorov, A., 1941. On the log-normal distribution of particles sizes during breakup process. Dokl. Akad. Nauk. XXXI, 99–101.

Lasheras, J.C., Hopfinger, E.J., 2000. Liquid Jet instability and Atomization in a Coaxial Gas Stream. Annu. Rev. Fluid Mech. 32, 275–308. URL: http://www.annualreviews.org/doi/10.1146/annurev.fluid.32.1.275, doi:doi:10.1146/annurev.fluid.32.1.275.

Lebas, R., Menard, T., Beau, P., Berlemont, A., Demoulin, F.X., 2009. Numerical simulation of primary break-up and atomization: DNS and modelling study. International Journal of Multiphase Flow 35, 247–260. URL: http://linkinghub.elsevier.com/retrieve/pii/S0301932208001821http://www.sciencedirect.com/science/article/pii/S0301932208001821, doi:doi:10.1016/j.ijmultiphaseflow.2008.11.005.

Lee, K., Girimaji, S.S., Kerimo, J., 2008. Validity of Taylor's dissipation-viscosity independence postulate in variable-viscosity turbulent fluid mixtures. Physical Review Letters 101, 1–4. doi:doi:10.1103/PhysRevLett.101.074501.

Lefèbvre, A.H., Lefebvre, A.H., Lefèbvre, A.H., Lefebvre, A.H., 1989. Atomization and Sprays. CRC Press.

Ling, Y., Fuster, D., Zaleski, S., Tryggvason, G., 2017. Spray formation in a quasiplanar gas-liquid mixing layer at moderate density ratios: A numerical closeup. Physical Review Fluids 2, 014005. URL: https://link.aps.org/doi/10.1103/PhysRevFluids.2.014005, doi:doi:10.1103/PhysRevFluids.2.014005.

Ling, Y., Fuster, D., Zaleski, S., Tryggvason, G., Zaleski, S., 2019. A two-phase mixing layer between parallel gas and liquid streams: multiphase turbulence statistics and influence of interfacial instability. Journal of Fluid Mechanics 859, 268–307. URL: https://www.cambridge.org/core/product/identifier/S002211201800825X/type/journal{_}article, doi:doi:10.1017/jfm.2018.825, arXiv:arXiv:1808.01996v1.

Lucci, F., Ferrante, A., Elghobashi, S., 2010. Modulation of isotropic turbulence by particles of Taylor length-scale size. Journal of Fluid Mechanics 650, 5–55. doi:doi:10.1017/S0022112009994022.

Manin, J., 2019. Numerical investigation of the primary breakup region of high-pressure sprays. Atomization and Sprays 28, 1081–1100. URL: http://dl.begellhouse.com/journals/6a7c7e10642258cc,forthcoming,26990.html, doi:doi:10.1615/AtomizSpr.2019026990.

Marmottant, P., Villermaux, E., 2004. On spray formation. Journal of Fluid Mechanics 498, 73–111. URL: http://www.journals.cambridge.org/abstract{_}S0022112003006529https://www.irphe.fr/{~}fragmix/publis/MV2004a.pdf, doi:doi:10.1017/S0022112003006529.

Park, G.I., Bassenne, M., Urzay, J., Moin, P., 2017. A simple dynamic subgrid-scale model for les of particle-laden turbulence. Physical Review Fluids 2, 1–20. doi:doi:10.1103/PhysRevFluids.2.044301.

Pope, S.B., 2001. Turbulent flows.

Popinet, S., 2009. An accurate adaptive solver for surface-tension-driven interfacial flows. J. Comput. Phys. 228, 5838–5866. URL: http://dx.doi.org/10.1016/j.jcp.2009.04.042, doi:doi:10.1016/j.jcp.2009.04.042.

Prakash, V.N., Martínez Mercado, J., Van Wijngaarden, L., Mancilla, E., Tagawa, Y., Lohse, D., Sun, C., 2016. Energy spectra in turbulent bubbly flows. Journal of Fluid Mechanics 791, 174–190. doi:doi:10.1017/jfm.2016.49, arXiv:1307.6252.

Roghair, I., Mercado, J.M., Sint Annaland, M.V., Kuipers, H., Sun, C., Lohse, D., 2011. Energy spectra and bubble velocity distributions in pseudo-turbulence: Numerical simulations vs. experiments. International Journal of Multiphase Flow 37, 1093–1098. URL: http://dx.doi.org/10.1016/j.ijmultiphaseflow.2011.07.004, doi:doi:10.1016/j.ijmultiphaseflow.2011.07.004.

Saddoughi, S.G., Veeravalli, V., S., Veeravalli, S.V., 1994. Local isotropy in turbulent boundary layers at high Reynolds number. Journal of Fluid Mechanics 268, 333–372. URL: http://www.journals.cambridge.org/abstract{_}S0022112094001370, doi:doi:10.1017/S0022112094001370.

Salvador, F., Ruiz, S., Crialesi-Esposito, M., Blanquer, I., 2018. Analysis on the Effects of Turbulent Inflow Conditions on Spray Primary Atomization in the Near-Field by Direct Numerical Simulation. International Journal of Multiphase Flow 102, 49–63. URL: http://linkinghub.elsevier.com/retrieve/pii/S0301932217305037, doi:doi:10.1016/j.ijmultiphaseflow.2018.01.019.

Scardovelli, R., Zaleski, S., 2003. Interface reconstruction with least-square fit and split Eulerian-Lagrangian advection. International Journal for Numerical Methods in Fluids 41, 251–274. doi:doi:10.1002/fld.431.

Schmidt, O.T., Towne, A., Rigas, G., Colonius, T., Brès, G.A., 2018. Spectral analysis of jet turbulence. Journal of Fluid Mechanics 855, 953–982. URL: http://arxiv.org/abs/1711.06296https://www.cambridge.org/core/product/identifier/S0022112018006754/type/journal{_}article, doi:doi:10.1017/jfm.2018.675, arXiv:1711.06296.

Shinjo, J., Umemura, A., 2010. Simulation of liquid jet primary breakup: Dynamics of ligament and droplet formation. International Journal of Multiphase Flow 36, 513–532. URL: http://linkinghub.elsevier.com/retrieve/pii/S0301932210000637, doi:doi:10.1016/j.ijmultiphaseflow.2010.03.008.

Taylor, G.I., 1935. Statistical theory of turbulence. Proceedings of the Royal Society of London. Series A, Mathematical and Physical Sciences 151, 421–444. URL: http://www.jstor.org/stable/96557, doi:doi:10.1098/rspa.1983.0054.

Uberoi, M.S., Freymuth, P., 1970. Turbulent energy balance and spectra of the axisymmetric wake. Physics of Fluids 13, 2205–2210. doi:doi:10.1063/1.1693225.

Villermaux, E., 2007. Fragmentation. Annual Review of Fluid Mechanics 39, 419–446. URL: http://www.annualreviews.org/doi/10.1146/annurev.fluid.39.050905.110214, doi:doi:10.1146/annurev.fluid.39.050905.110214.

Wang, Y., Bourouiba, L., 2018. Unsteady sheet fragmentation: Droplet sizes and speeds. Journal of Fluid Mechanics 848, 946–967. doi:doi:10.1017/jfm.2018.359.

Zandian, A., Sirignano, W.A., Hussain, F., 2018. Understanding liquid-jet atomization cascades via vortex dynamics. Journal of Fluid Mechanics 843, 293–354. doi:doi:10.1017/jfm.2018.113, arXiv:1706.03742.